Nanoscale

Accepted Manuscript

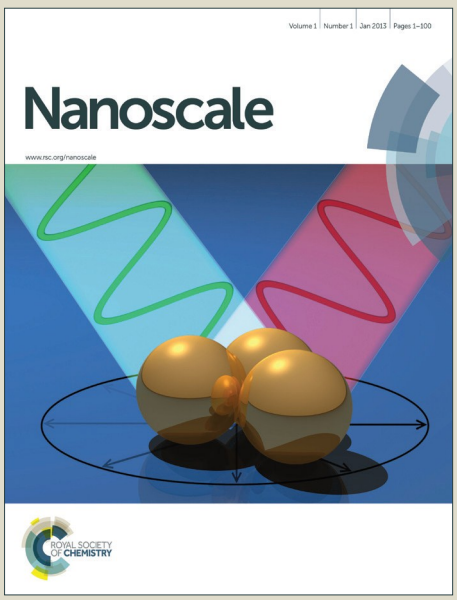

ROYAL SOCIETY OF CHEMISTRY

www.rsc.org/nanoscale

Nanoscale

RSC Publishing

ARTICLE

Carbon quantum dots decorated Cu_2S nanowire arrays for enhanced photoelectrochemical performance

Cite this: DOI: 10.1039/xoxxoooooox

Received ooth January 2015,
Accepted ooth January 2015

DOI: 10.1039/xoxxoooooox

www.rsc.org/

Ming Li,[a] Renjie Zhao,[a] Yanjie Su,*[a] Zhi Yang,[a] and Yafei Zhang*[a]

The photoelectrochemical (PEC) performance of Cu_2S nanowire arrays (NWAs) has been demonstrated to be greatly enhanced by dipping-assembly of carbon quantum dots (CQDs) on the surfaces of Cu_2S NWAs. Experimental results show that the pristine Cu_2S NWAs with higher aspect ratios exhibit better PEC performance due to the longer length scale for light absorption and the shorter length scale for minority carrier diffusion. Importantly, the CQDs decorated Cu_2S NWAs exhibit remarkably enhanced photocurrent density, giving a photocurrent density of 1.05 mA cm^{-2} at 0 V *vs* NHE and an optimal photocathode efficiency of 0.148% under illumination of AM 1.5G (100 mW cm^{-2}), which is 4 times higher than that of the pristine Cu_2S NWAs. This can be attributed to the improved electron transfer and the energy-down-shift effect of CQDs. We believe that this inexpensive Cu_2S/CQDs photocathode with increased photocurrent density opens up new opportunities in PEC water splitting.

Introduction

Due to the growing global energy consumption and increasing concern for environmental issues, solar water splitting for hydrogen production has attracted significant attention as method for generating carbon-free fuels from solar energy.[1] Photoelectrochemical (PEC) water splitting is one of the most attractive approaches to produce hydrogen in an eco-friendly manner with no carbon emission, which requires only semiconductor electrodes, water and sunlight.[2-5] Since the pioneering work by Fujishima and Honda in the early 1970s,[6] PEC water splitting using semiconductor materials as photoelectrodes has been intensively studied to obtain efficient solar-to-hydrogen conversion in the past forty years. While much attention has been devoted to photoanode materials (*e.g.*, TiO_2, ZnO, Fe_2O_3, WO_3),[7-12] the development of the PEC tandem cell is limited by the identification of stable and inexpensive *p*-type photocathode materials.[13] Furthermore, they are advantageous over *n*-type ones in terms of hydrogen generation as the photo-generated electrons can be directly injected into the electrolyte on the *p*-type semiconductors and thus directly reduce water to hydrogen at the semiconductor/water interface without potential energy loss.[14]

As a *p*-type semiconductor with metal vacancies in the lattice, Cu_2S has an indirect band gap of 1.2 eV, which can be considered as an ideal sunlight absorbing material for solar cells and corresponds to a maximum theoretical efficiency of 30%.[15,16] Historically, the CdS/Cu_2S heterojunction photovoltaic devices reached efficiencies near 10%, which had been competitive with planar silicon-based photovoltaics.[17,18] Although the bandgap of Cu_2S is too small to split water, this inexpensive, earth-abundant and industrial mature semiconductor has many attractive features as a photocathode material for PEC water splitting, including a suitable bandgap that enables much solar light absorption and a conduction band energy level suitable for hydrogen generation.[19,20] Compared with those of bulk materials, it is known that semiconductor nanowire arrays (NWAs) have the capability of independently modulating an actual carrier diffusion length and light absorption depth and the advantages of enhanced light trapping, reduced light reflection, improved band gap tuning, facile strain relaxation and increased structure defect tolerance.[21,22] These advantages indicate that the NWAs geometry is an ideal structure to resolve the mismatch between the short minority carrier diffusion length and the longer light absorption length in Cu_2S by decoupling these directions.[23,24] Moreover, compared to thin film and bulk structure, the NWAs have higher specific surface areas, thus increasing the electrode/electrolyte interface for electrochemical reactions in PEC water splitting.[25,26] Therefore, the Cu_2S NWAs may eventually lead to the overall goal of high efficient and scalable PEC photocathodes.

To date, various methods have been used to synthesize the Cu_2S NWAs.[27-30] Among them, the gas-solid reaction is considered as a cost-effective, easy scaled-up method to prepare large-area Cu_2S NWAs on Cu foil or film substrates.[31] In the reaction, the NWAs are self-grown from a Cu substrate without any catalysts or templates at room temperature.[29-31] The

Cu foil or film as a precursor can promote the growth of Cu_2S NWAs and also be used as an electrode when the Cu_2S NWAs are applied to PEC cells.[29] Yang *et al.*[20] first investigated the PEC performance of Cu_2S NWAs grown on a Cu foil, and demonstrated that the cathodic photocurrent of 0.11 mA cm^{-2} at -0.5V *vs* Ag/AgCl can be increased to 0.14 mA cm^{-2} by coating a CdS shell layer on the nanowire surface. Ren *et al.*[31] introduced that the diameters and lengths of Cu_2S nanowires had a great impact on the light absorption abilities. However, the influence of morphology of the self-grown Cu_2S NWAs on the PEC performance has not yet been systematically investigated. Additionally, the photocurrent of the CdS nanoparticles decorated Cu_2S NWAs photocathode is still too low to compete with other NWAs photocathodes (*e.g.*, Cu_2O and CuO).[14,25]

Recently, carbon quantum dots (CQDs) have been widely used to modify semiconductor nanostructures, such as Si nanowires,[32,33] Cu_2O microspheres,[34] TiO_2 nanostructures,[35-39] $BiVO_4$ inverse opal structures,[40] $SrTiO_3$ nanoparticles,[41] and Bi_2O_3 inverse opal structures,[42] by which the photocatalytic and photoelectric properties can be remarkably enhanced due to the strong size and excitation wavelength-dependent photoluminescence behaviour, broad band optical absorption, and high electrical conductivity of CQDs.[43] Enlightened by this, it is easy to come up with the idea of improving the PEC performance of Cu_2S NWAs by attaching CQDs.

Herein, we report the self-grown of the Cu_2S NWAs on Cu foil surface and the dipping-assembly of CQDs on the Cu_2S NWAs as photocathodes. CQDs were used as sensitizer to enhance the PEC performance of Cu_2S NWAs. To obtain an optimal template for CQDs modification, the influence of nanowire morphology on the PEC performance of Cu_2S NWAs photocathode was investigated. The effect of CQDs loading on the surfaces of Cu_2S nanowires was also investigated to optimize the photocurrent and its stability. An energy band diagram was also proposed to help illustrating the working mechanism of the improved PEC performance for the Cu_2S/CQDs NWAs photocathode.

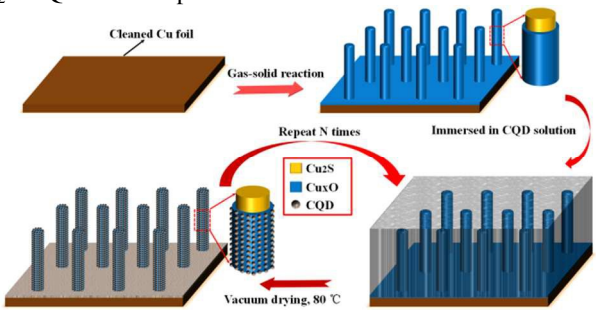

Scheme 1 Schematic illustration of the preparation of Cu_2S/CQDs NWAs.

Experimental

Synthesis of Cu_2S NWAs

The Cu_2S NWAs were synthesized by gas-solid reaction method. Firstly, Cu foil (99.9% purity, ~4×4 cm) was carefully polished with abrasive paper (2000 mesh) and ultrasonically washed using deionized water and ethanol. The cleaned Cu foil was then placed into an airtight stainless steel reactor to performing the gas-solid reaction (as shown in **Scheme S1**). Secondly, a mixed gas of H_2S and O_2 at a volume ratio of 2:1 was introduced into the reactor for 1 min, which was then sealed and kept at a fixed temperature of 20-30 °C for different times. As the Cu surface became black and fluffy, dense Cu_2S NWAs were grown on the surface.

Synthesis of Cu_2S/CQDs NWAs

The Cu_2S/CQDs NWAs were fabricated by assembling CQDs on the surfaces of Cu_2S NWAs via a dipping-assembly method,[33] as shown in **Scheme 1**. A certain volume of CQDs solution (detailed synthesis process and properties of CQDs in Supporting Information)[44] was dropped on the surfaces of Cu_2S NWAs (0.5 ml/cm^2), which was then dried in vacuum at 80 °C for 2 hours. The cycle times were used to control the amounts of CQDs, and the Cu_2S/CQDs-x NWAs were obtained, where x represents the deposition cycles of CQDs.

Characterization

The morphologies of the samples were characterized by a field emission scanning electron microscopy (FE-SEM, Carl Zeiss Ultra 55, Germany) operating at 20 kV. Transmission electron microscopy (TEM, JEM-2100, JEOL, Japan) operating at 200 kV was used to observe the microstructures of the samples. The crystalline structure of the samples was analysed by X-ray diffraction (XRD) using an advanced X-ray diffractometer (D8 ADVANCE, Bruker, Germany) in the diffraction angle range 2θ = 20-60°, with Cu Kα radiation (λ = 0.154056 nm) at voltage of 40 kV and a current of 40 mA. The X-ray photoelectron spectra (XPS) were acquired using a Japan Kratos Axis UltraDLD spectrometer with a monochromatic Al Kα source (1486.6 eV).The UV-vis-NIR absorption and diffuse reflectance spectra (DRS) were carried out using a UV-vis-NIR spectrophotometer (Lambda 950, PerkinElmer, USA). The photoluminescence (PL) spectra were obtained with a fluorescence spectrophotometer (F-4600, Hitachi, Japan). Fourier transform infrared (FTIR) spectra were recorded on a VERTEX 70 spectrometer (Bruker, Germany). The Raman spectra were acquired by using a dispersive Raman microscope (Senterra R200-L, Bruker Optics, Germany), operated with a 532 nm laser.

PEC measurements

To perform the PEC tests, the Cu substrates of the NWAs were connected with enamelled Cu wire through high-purity silver conducting paint. To prevent photocurrent leakage, the edges and backside of samples were sealed using epoxy resin, excluding an area of 1.0 cm^2 for absorbing the light. For easy measurement, the samples were fixed on glass slides by epoxy resin. A three-electrode PEC cell using a 200 mL aqueous solution of 1.0 M KCl (pH = 5.97) was used to carry out the current density measurements. The sample as working electrode (WE), Pt net as counter electrode (CE) and Ag/AgCl (saturated

KCl) as reference electrode (RE) were the three electrodes in the PEC cell. Illumination was provided by a solar simulator (CHF-XM500, Beijing Perfectlight) using a 500 W Xenon lamp and equipped with AM 1.5G filter. Light power intensity was maintained at 100 mW cm^{-2} at the sample position. An electrochemical workstation (CHI 650E) was used to measure current-voltage characteristics of the photocathodes under chopped light irradiation (light on/off cycle: 5s), with a scan rate of 5 mV S^{-1}. The PEC stability of the samples was evaluated by measuring the photocurrent densities produced under chopped light irradiation (light on/off cycle: 5s) at a fixed electrode potential of -0.25 V *vs* Ag/AgCl (0.2 V *vs* RHE).

The measured potentials versus the Ag/AgCl RE were converted to the RHE scale via the Nernst eqn.:

$$E_{RHE} = E_{Ag/AgCl} + 0.059\ pH + E_0$$

where E_{RHE} is the converted potential versus RHE, $E_{Ag/AgCl}$ is the experimental potential measured against the Ag/AgCl RE, and E_0 is the standard potential of Ag/AgCl (saturated KCl) at 25 °C (*i.e.*, 0.197).

Electrochemical impedance spectroscopy (EIS) in Nyquist plot of the samples was performed in 1.0 M KCl aqueous solution at open circuit potential. The amplitude of the sinusoidal wave was set at 5 mV, and the frequency varied from 10 kHz to 0.1 Hz.

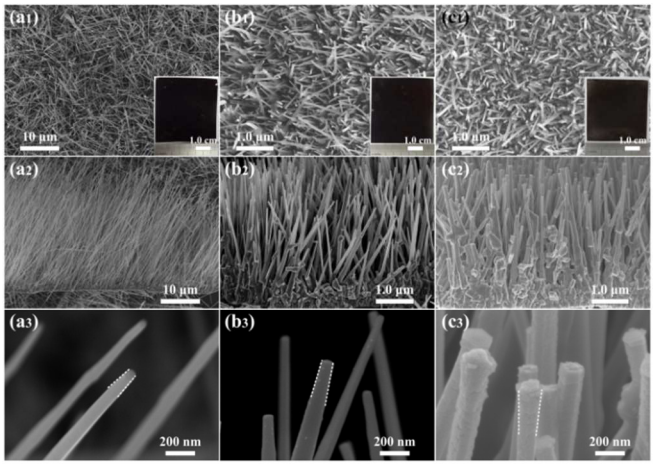

Fig. 1 SEM images of the Cu_2S NWAs grown at different temperatures: (a_1-a_3) 20, (b_1-b_3) 25 and (c_1-c_3) 30 °C. Insets: optical images of the corresponding samples.

Results and discussion

Fig. 1 shows the typical morphologies of the Cu_2S NWAs under different temperatures. It can be concluded that the relatively lower reaction temperature results in smaller average diameter, larger average length, higher density and darker sample colour. For example, the Cu_2S NWAs prepared at 20 °C possess an average diameter of 88 nm and an average length of 28 μm, whereas those prepared at 30 °C have an average diameter of 200 nm and an average length of 4.3 μm. It is also found that lower temperature (20-25 °C) is beneficial to the formation of base-tapered nanowires (**Fig. 1a_3-c_3**). Furthermore, prolonging the reaction time can also be used to prepare Cu_2S nanowires with long lengths and large diameters (**Fig. S2**).The detailed relationship between the preparation conditions (reaction temperature and time) and the diameter, length and spacing density of the Cu_2S NWAs are presented in **Table S1**. The results suggest that both relatively lower reaction temperature and longer reaction time are beneficial to the growth of Cu_2S nanowires with high aspect ratios.

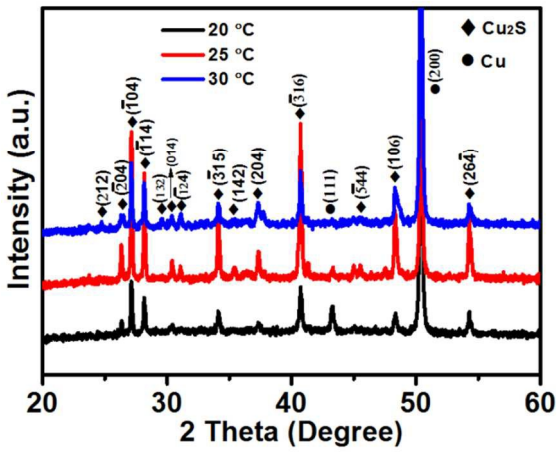

Fig. 2 XRD patterns of Cu_2S NWAs grown at different temperatures.

The XRD patterns of the Cu_2S NWAs grown at different temperatures are shown in **Fig. 2**. The diffraction peaks can be indexed as monoclinic Cu_2S (JPCDS no. 33-0490). The EDS result (**Fig. S3**) shows that the nanowires are composed of Cu, S, and O, indicating the existence of CuxO (x = 1, 2), which is confirmed by the Raman analysis (**Fig. S4**).[45-47]

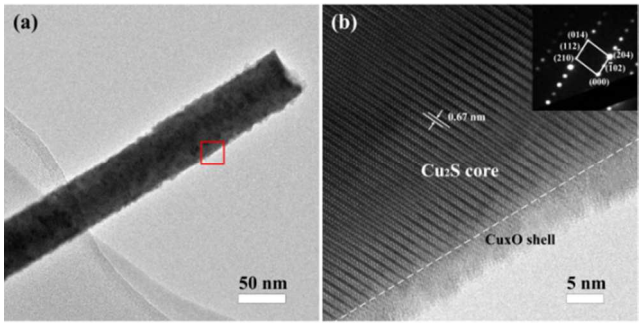

Fig. 3 (a) TEM image of a Cu_2S nanowire. (b) HRTEM image of the region marked in (a). Inset: SAED pattern for Cu_2S core.

The TEM image of a single Cu_2S nanowire is shown in **Fig. 3a**, exhibiting its rough surface and a diameter of ~56 nm. From high-resolution TEM (HRTEM) image (**Fig. 3b**), it can be clearly seen that the nanowire surface is covered with a thin CuxO layer having a thickness of ~6 nm and low crystallinity to form a core/shell nanowire structure. The calculated lattice spacing of the core is ~0.67 nm corresponding to the interplanar distance of the $(\bar{1}02)$ crystal plane of monoclinic Cu_2S, which is consistent with that reported elsewhere for the Cu_2S nanowires using the same method.[29-31] The selected-area electron diffraction (SAED) pattern (inset, **Fig. 3b**) confirms

that the Cu_2S single crystallinity is oriented along the $(\bar{1}02)$ direction.

As show in **Fig.4**, all Cu_2S NWAs synthesized at different temperatures show excellent light absorption abilities over a wide range of the wavelengths from 250 to 850 nm. The Cu_2S NWAs grown at lower reaction temperature exhibit better light absorption, which can be ascribed to the longer lengths and base-tapered morphologies.[31,48] The Cu_2S NWAs prepared at 20 °C exhibit 93.1-99.7 % absorbance over the wavelength range of 250-850 nm. The average absorbance can reach to 99.2 % at 550 nm wavelength. This excellent light trapping ability can attribute to not only the geometry of Cu_2S NWAs but also their optimal bandgap for light absorption. As shown in the insets of **Fig. 4** and **Fig. S5**, the bandgap of Cu_2S NWAs is estimated to be ~1.25 eV, which is larger than that of the corresponding bulk material (1.20 eV). The result is consistent with the previous reported Cu_2S NWAs using the same method.[31] For one thing, the naturally formed CuxO shell layer can increase the bandgap of Cu_2S nanowires probably due to its relatively larger bandgap (E_g (CuO) = 1.4 eV, E_g (Cu_2O) = 2.0 eV)[14,25] than Cu_2S. For another thing, the increased surface-to-volume ratio of Cu_2S NWAs compared with planar structure will result in increased CuxO amount.

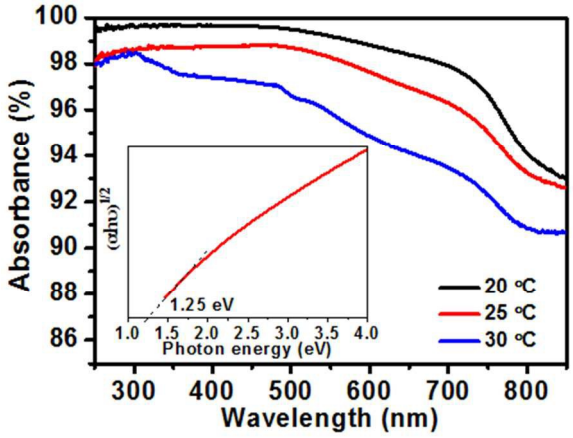

Fig. 4 Absorbance of the Cu_2S NWAs grown at different temperatures. Inset: energy band gap determination of the Cu_2S NWAs grown at 25 °C.

Although the Cu_2S NWAs with high aspect ratios exhibit better light absorption ability, they are easy to fall over after dipping-assembly of CQDs (**Fig. S6**). For this reason, we chose NWAs grown at 25 °C as templates to fabricate Cu_2S/CQDs NWAs. **Fig. 5a** shows a typical SEM image of Cu_2S NWAs after dipping-assembly of CQDs for 4 cycles. It can be observed that the tips of adjacent nanowires are aggregated together by CQDs (**Fig. 5b**). The FTIR (**Fig. 5c**) and EDS spectra (**Fig. S7**) confirm the formation of Cu_2S/CQDs NWAs. However, the traces of CQDs cannot be distinguished from the image due to the resolution limit of SEM. TEM image (**Fig. 5d**) of the Cu_2S/CQDs-4 nanowires show that the CQDs have been successfully decorated on the surfaces of Cu_2S nanowires as the nanoparticle sizes are consistent with that of the pristine CQDs (3-9 nm, **Fig. S1a**). The HRTEM image (**Fig. 5e**) demonstrates that the monocrystalline Cu_2S core was uniformly coated by a thin CuxO shell layer with thickness of ~10 nm and low crystallinity, and the traces of CQDs marked by the white dotted round frames can be observed. From the HRTEM image of the top of a Cu_2S/CQDs-4 nanowire (**Fig. 5f**), many amorphous CQDs can also be found. Furthermore, the EDS elemental mapping (**Fig. 5g-j**) for a segment of Cu_2S/CQDs-4 nanowire suggest that the CQDs are evenly distributed on the surfaces of the Cu_2S nanowires.

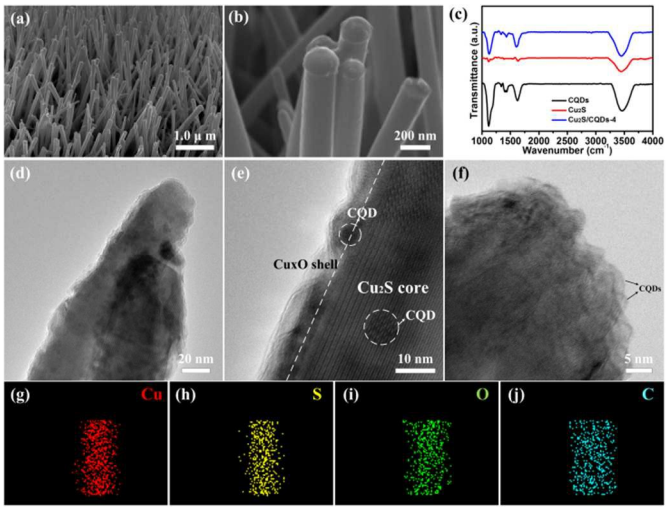

Fig. 5 (a) and (b) SEM images of Cu_2S/CQDs-4 NWAs. (c) FTIR spectra of CQDs, Cu_2S and Cu_2S/CQDs-4 nanowires. (d) TEM image of Cu_2S/CQDs-4 nanowires. HRTEM images of the (e) trunk and (f) top of a Cu_2S/CQDs-4 nanowire. Elemental mapping of (g) Cu, (h) S, (i) O and (j) C for a segment of Cu_2S/CQDs-4 nanowire.

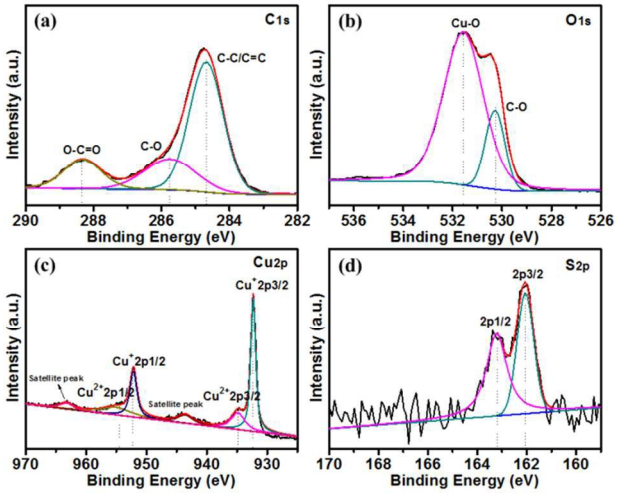

Fig. 6 XPS spectra of Cu_2S/CQDs-4 NWAs: (a) C 1s, (b) O 1s, (c) Cu 2p and (d) S 2p.

XPS was used to further characterize the Cu_2S/CQDs-4 NWAs as shown in **Fig. 6**. The deconvoluted C1s region (**Fig. 6a**) shows different carbon functionalities. The typical peaks at 284.7, 285.8 and 288.3 eV can be attributed to the C-C/C=C, C-

O and O-C=O bonds, respectively.[49] The peaks at 530.3 and 531.5 eV in the deconvoluted O1s XPS spectrum are assigned to the Cu-O and C-O, respectively (**Fig. 6b**). The XPS spectra of Cu 2p (**Fig. 6c**) and S 2p (**Fig. 6d**) suggest the co-existence of CuO and Cu_2O on the surfaces of Cu_2S nanowires.[31]

Although the CQDs possess excellent abilities to absorb ultraviolet light (**Fig. S1c**), there is no big difference between Cu_2S and Cu_2S/CQDs-4 NWAs in light absorption (**Fig. S8**). There are two possible reasons for this phenomenon: One is that the aggregation of adjacent nanowires will lead to light absorption deterioration of NWAs, which can be compensated by the CQDs. The other one is that the influence of CQDs on the improvement of light absorption may be covered by that of Cu_2S NWAs as they also exhibit excellent light trapping ability in the ultraviolet region.

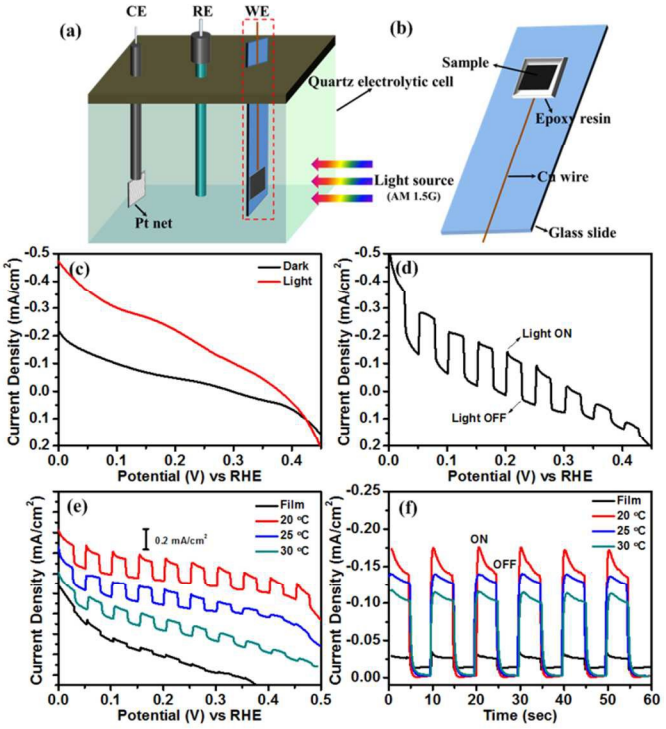

Fig. 7 (a) Schematic PEC setup using the NWAs as working electrodes. (b) Schematic illustration of the construction of a photocathode. LSV curves of the Cu_2S NWAs prepared at 25 °C (c) at dark and illumination, and (d) under chopped illumination. (e) LSV curves of the Cu_2S NWAs prepared at different conditions under chopped illumination. (f) Amperometric *I-t* curves of the corresponding samples at 0.2 V *vs* RHE under chopped illumination.

The PEC measurements were carried out in a three-electrode configuration with the NWAs photocathode (**Fig. S9**), Ag/AgCl electrode, and Pt net as the WE, RE and CE, respectively, as illustrated in **Fig. 7a**, **b**. **Fig. 7c** shows the linear sweep voltammetry (LSV) curves at dark and under illumination for the Cu_2S NWAs grown at 25 °C. It can be seen that the NWAs exhibit obvious photocurrent under light illumination, implying that efficient charge generation and separation happened at the semiconductor/electrolyte interface. When the illumination is chopped with a frequency of 0.2 Hz during the LSV scan, the dark and light currents could be simultaneously monitored, as show in **Fig. 7d**. Obviously, the absolute photocurrent decreases as bias potential decreases.

As shown in **Fig. 7e**, all Cu_2S NWAs prepared at different temperatures exhibit higher photocurrent response than the Cu_2S film prepared with the same method. In addition, the Cu_2S NWAs with higher aspect ratios prepared at lower temperature demonstrate better PEC performance. The enhanced photocurrent density can be ascribed to the fact that the increased light absorption results in the generation of more photo-generated carriers and the decreased nanowire diameter is more favourable to electron transfer. **Fig. 7f** illustrates the transient current density under chopped illumination for the corresponding samples at 0.2 V *vs* RHE, exhibiting good switching behaviour and stability of Cu_2S NWAs. The photocurrent density of Cu_2S NWAs can reach 0.175 mA cm^{-2}, which is about 9 times larger than that of the film sample (0.02 mA cm^{-2}), demonstrating the superiority of NWAs geometry.

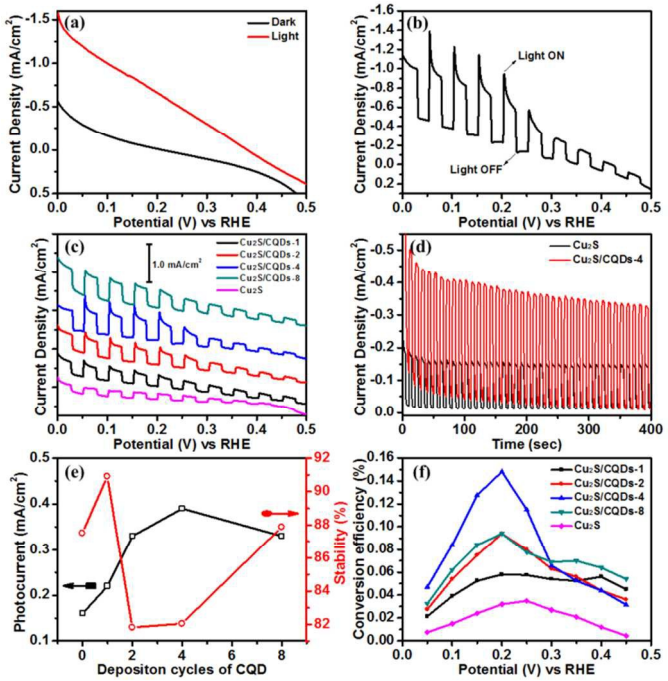

Fig. 8 LSV curves of the Cu_2S/CQD-4 NWAs (a) at dark and under illumination, and (b) under chopped illumination. (c) LSV curves of the Cu_2S/CQDs-x NWAs under chopped illumination. (d) Amperometric *I-t* curves of the Cu_2S and Cu_2S/CQDs-4 NWAs at 0.2 V *vs* RHE under chopped illumination. (e) Photocurrent densities and stabilities (measured at 0.2 V *vs* RHE) of the Cu_2S/CQDs-x NWAs as a function of deposition cycle of CQDs. (f) Photoconversion efficiencies *vs* applied bias potential for the Cu_2S/CQDs-x NWAs.

The effect of the CQDs amount on the PEC performace of Cu_2S/CQDs NWAs was also investigated by changing assemblying cycles. **Fig. 8a** shows the LSV curves of the Cu_2S/CQDs-4 NWAs at dark and under illumination. It is

obvious that the photocurrent has been greatly increased compared with that of the pristine Cu_2S NWAs (**Fig. 7a**). The maximum photocurrent of the Cu_2S/CQDs-4 NWAs at 0 V *vs* RHE has reached 1.05 mA cm^{-2}, which is about 4 times larger than that of the Cu_2S NWAs (0.26 mA cm^{-2}). The LSV curve of the Cu_2S/CQDs-4 NWAs under chopped illumination also confirms the greatly enhanced photocurrent response, as shown in **Fig. 8b**. The photocathode current overshoots in the beginning of switching light on can be ascribed to the accumulation of photogenerated carriers at the interface between composite nanowires and electrolyte.[50] The enhanced photocurrent demonstrates that the CQDs are good acceptors for electron transfer from nanowire to electrolyte.[34,49] **Fig. 8c** shows the photocurrent of Cu_2S/CQDs-x photocathodes with different assemblying cycles (x = 1, 2, 4 and 8), and the corresponding absolute photocurrent densities are calculated as shown in **Fig. S10**. The results indicate that the photocurrent densities of the Cu_2S/CQDs photocathodes first increase with increasing CQDs amounts and reach a peak at 4 cycles before declining thereafter. The deteriorated PEC performance for the NWAs with thicker CQDs layer (Cu_2S/CQDs-8) can be ascribed to the hindered electron migration.[14,39]

The stability of the photocathodes under illumination is evaluated with chronoamperometric measurements at 0.2 V *vs* RHE in chopped light with a frequency of 0.2 Hz over 400 s. The stability is quantified as the percentage of the photocurrent density at the end of the last light cycle compared with that at the end of the first cycle within the 400 s measurement period. A close comparison of the photocurrent density decay curves of the pristine Cu_2S and Cu_2S/CQDs-4 NWAs photocathodes is presented in **Fig. 8d**. Compared with the stability of 87.5% for the Cu_2S NWAs photocathode, the Cu_2S/CQDs-4 NWAs photocathode shows a slightly decreased stability of 82.1%. To investigate the reason for the deteriorated stability, the photocurrent stability of other Cu_2S/CQDs NWAs photocathodes was also characterized (**Fig. S11**). The results are summarized in **Table S2** and presented in **Fig. 8e**. Obviously, the Cu_2S/CQDs-1 NWAs exhibit a slightly increased stability of 90.9% compared with that of pristine Cu_2S NWAs, indicating that CQDs themselves can improve the stability of NWAs. However, when the deposition cycle of CQDs is increased to 2, the stability for Cu_2S/CQDs-2 is greatly decreased to 81.8%, which may result from the poor physical adsorption ability between the assembled CQDs in electrolyte.[51] Further increasing the deposition cycle of CQDs, the stability can be improved to 82.1% for Cu_2S/CQDs-4 NWAs and 87.9% for Cu_2S/CQDs-8. The results indicate that an optimal CQDs layer on Cu_2S nanowires can be used to improve the photocurrent and maintain the relatively high stability as well.

The photoconversion efficiencies of the Cu_2S/CQDs NWAs photocathodes were calculated with following the equation of $\eta = JV/P_{in}$,[14,52] where J and V are the photocurrent density (**Fig. S10**) and photovoltage (V *vs* RHE) and P_{in} (mW cm^{-2}) is the incoming light flux (100 mW cm^{-2}). **Fig. 8f** presents the plots of the photoconversion efficiencies versus applied bias potentials for the Cu_2S/CQDs NWAs. It can be observed that all Cu_2S/CQDs NWAs show greatly enhanced photoconversion efficiencies compared with the pristine Cu_2S NWAs. Their optimal conversion efficiencies are summarized in **Table S2**. As a result, the Cu_2S/CQDs-4 NWAs exhibit the highest conversion efficiency of 0.148 %, which is about 4 times larger than that of the pristine Cu_2S NWAs (0.035%).

After 30 min PEC water splitting process at 0.2 V *vs* RHE, the surfaces of Cu_2S and Cu_2S/CQDs-4 nanowires became rougher as a result of photocorrosion (**Fig. S12 a_1, b_1**). The increase in oxygen (**Fig. S12 a_2, b_2**) demonstrates that CuxO nanoparticles may form on the surfaces of nanowires. Although the Cu_2S/CQDs-4 NWAs exhibit improved ability against photocorrosion compared with the pristine Cu_2S NWAs, the main challenge to use the Cu_2S/CQDs NWAs for practical hydrogen production is long-term stability since both the Cu_2S nanowires and the assembled CQDs are not stable over long time.[21,51]

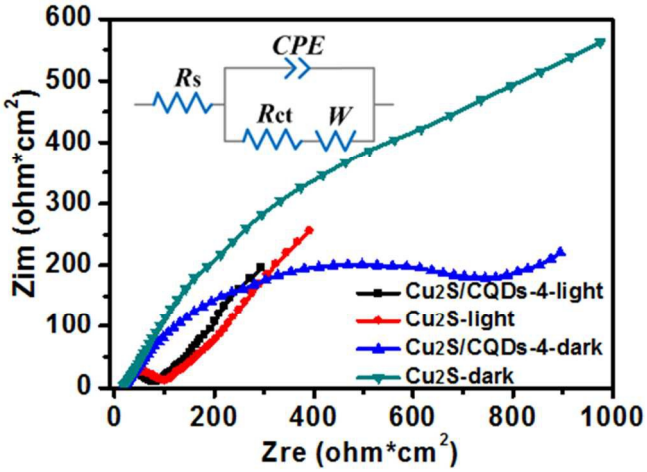

Fig. 9 Nyquist plots (Z_{re} *vs* Z_{im}) of the Cu_2S and Cu_2S/CQDs-4 NWAs at dark and under illumination.

Impedance measurements were also performed to study the enhanced PEC properties of the Cu_2S/CQDs NWAs.[40] **Fig. 9** presents the Nyquist plots of the Cu_2S and Cu_2S/CQDs-4 NWAs at dark and under illumination. All Nyquist plots display a semicircle at high frequencies whose diameter represents the charge transfer resistance (R_{ct}), which controls the electron transfer kinetics of the redox probe at the electrode interface.[14] The straight line at low frequency is related to the diffusion process. The corresponding equivalent circuit is depicted in the inset of **Fig. 9**, where R_s denote the bulk resistance, originating from the electrolyte and the electrode, *CPE* is the constant phase element that models capacitance of the double layer, and *W* stands for the Warburg impedance originated from the diffusion process at the electrode surface. It is evident that the R_{ct} at dark is larger than that under light illumination for both kinds of photocathodes. Additionally, the Cu_2S/CQDs photocathode shows a lower R_{ct} value than the pristine Cu_2S photocathode both at dark and under illumination. The fitting results of R_{ct} for the Cu_2S/CQDs-4 NWAs at dark and under illumination are 665.1 and 70.1 Ω cm^2, respectively, which are

smaller than the corresponding values of the pristine Cu_2S NWAs (992.0 and 94.6 Ω cm^2 at dark and under illumination, respectively). The results demonstrate that the CQDs facilitate the electron transfer from Cu_2S nanowire to the electrolyte, and the reduced R_{ct} is also correlated with the enhanced PEC performance.

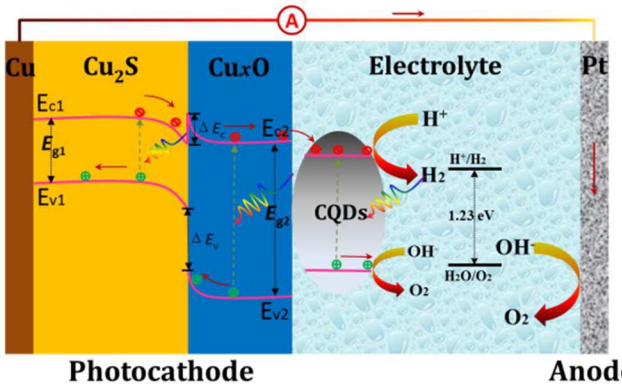

Scheme 3 Proposed mechanism of PEC water splitting and energy level distribution of different components.

The PEC water splitting mechanism and charge transfer process in Cu_2S/CQDs NWAs photocathode can be illustrated in **Scheme 3**. As both the conduction band minimum (CBM) and valence band maximum (VBM) of Cu_2S are higher than those of CuO, type-II heterostructure of Cu_2S/CuO can form to promote the separation of the photo-generated carriers.[53-56] Although the CBM of Cu_2O is just a little higher (0.25 eV) than that of Cu_2S,[53,54] it is reasonable to expect Cu_2O to have electron accepting properties for the Cu_2S/Cu_2O heterostructure because conduction band barriers smaller than 0.3-0.4 eV do not impose a problem for current transport in ~1.2 eV band gap devices.[57,58] Additionally, the Cu_2O/CuO has also been demonstrated to be an efficient type-II heterostructure for electron transfer.[55,59] Consequently, the Cu_2S/CuxO heterojunction should be efficient for PEC water splitting. Moreover, the CQDs in Cu_2S/CQDs NWAs play dual important roles for the improved PEC performance. Firstly, under illumination, the decorated CQDs serve as electron sinks that suppress the recombination of photo-generated carriers and then facilitate the electron transfer from Cu_2S/CuxO to the electrolyte to reduce water and form H_2 under the external bias potential. Secondly, the CQDs possess excellent abilities to absorb ultraviolet light (**Fig. S1c**). On the one hand, the corresponding photo-generated electrons can be used to reduce water directly. On the other hand, the excited-state CQDs can emit longer wavelength light as a result of down conversion (**Fig. S1d**),[60] which in turn excites Cu_2S to form electron/hole pairs to some extent, which also participate in PEC water splitting.

Conclusions

In summary, we have demonstrated a photocathode design for PEC water splitting by the dipping-assembly of CQDs on the Cu_2S NWAs. Experimental results show that the Cu_2S NWAs with higher aspect ratios show relatively higher PEC performance. More importantly, decorating the Cu_2S NWAs with CQDs can further enhance the photocurrent density, and the Cu_2S/CQDs NWAs shows an optimal PEC performance, producing a photocurrent density of 1.05 mA cm^{-2} at 0 V *vs* NHE and an optimal photocathode efficiency of 0.148%, which is 4 times higher than that of the pristine Cu_2S NWAs. This enhancement can be ascribed to the improved electron transfer and the energy-down-shift effect of CQDs. This Cu_2S/CQDs NWAs photocathode promises to have a great potential in the construction of low-cost and high performance PEC cells.

Acknowledgements

This work was supported by National High Technology Research and Development Program of China (No.2011AA050504), National Natural Science Foundation of China (No. 51402190, No. 61574091), Shanghai Natural Science Foundation (No. 13ZR1456600), the Program of Shanghai Academic/ Technology Research Leader (15XD1525200) and the Program for Professor of Special Appointment (Eastern Scholar) at Shanghai Institutions of Higher Learning. We also acknowledge the analysis support from the Center for Advanced Electronic Materials and Devices the Instrumental Analysis Center of SJTU.

Notes and references

[a] *Key Laboratory for Thin Film and Microfabrication of the Ministry of Education, Department of Micro/Nano Electronics, School of Electronics, Information and Electrical Engineering, Shanghai Jiao Tong University, Shanghai 200240, PR China. Tel:+86-021-34205665; Fax: +86-021-34205665; Email: yanjiesu@sjtu.edu.cn, yfzhang@sjtu.edu.cn*

†*Electronic Supplementary Information (ESI) available: detailed synthesis process and properties of CQDs, the synthesis and characterization of pristine Cu_2S NWAs* and detailed amperometric I-t curves of the Cu_2S/CQDs-x NWAs. *See DOI: 10.1039/b000000x/*

1 M. Grätzel, *Nature*, 2001, **414**, 338−344.
2 T. Hisatomi, J. Kubota and K. Domen, *Chem. Soc. Rev.*, 2014, **43**,7520−7535.
3 P. Wang, Y. H. Ng and R. Amal, *Nanoscale*, 2013, **5**, 2952−2958.
4 X. Sun, Q. Li, J. Jiang and Y. Mao, *Nanoscale*, 2014, **6**, 8769−8780.
5 S. Lee, S. Park, G. S. Han, D. H. Kim, J. H. Noh, I. S. Cho, H. S. Jung and K. S. Hong, *Nanoscale*, 2014, **6**, 8649−8655.
6 A. Fujishima and K. Honda, *Nature*, 1972, **238**, 37-38.
7 Z. Zhang and P. Wang, *Energy Environ. Sci.*, 2012, **5**, 6506−6512.
8 Y. Liu, H. Zhou, J. Li, H. Chen, D. Li, B. Zhou and W. Cai, *Nano-Micro Lett.*, 2010, **2**, 277−284.
9 N. T. Hahn, H. Ye, D. W. Flaherty, A. J. Bard and C. B. Mullins, *ACS Nano*, 2010, **4**, 1977−1986.
10 Y. Liu, Y. Jiao, H. Y. Zhou, X. Yu, F.Y. Qu and X. Wu, Nano-Micro Lett., 2015, **7**, 12−16.
11 M. Choi and K. Yong, *Nanoscale*, 2014, **6**, 13900−13909.
12 T. Wang, Z. Jiao, T. Chen, Y. Li, W. Ren, S. Lin, G. Lu, J. Ye and Y. Bi, *Nanoscale*, 2013, **5**, 7552−7557.
13 L. Rovelli, S. D. Tilley and K. Sivula, *ACS Appl. Mater. Interf.*, 2013, **5**, 8018-8024.

14 Z. Zhang, R. Dua, L. Zhang, H. Zhu, H. Zhang and P. Wang, *ACS Nano*, 2013, **7**, 1709–1717.
15 A. Rothwarf, *Sol. Cells*, 1972, **2**, 115–140.
16 C. H. Henry, *J. Appl. Phys.*, 1980, **51**, 4494–4500.
17 J. A. Bragagnolo, A. M. Barnett, J. E. Phillips, R. B. Hall, A. Rothwarf and J. D. Meakin, *IEEE Trans. Electron Devices*, 1980, **27**, 645–651.
18 S. C. Riha, S. Jin, S. V. Baryshev, E. Thimsen, G. P. Wiederrecht and A. B. F. Martinson, *ACS Appl. Mater. Interf.*, 2013, **5**, 10302–10309.
19 Y. Zhao, N. C. Anderson, K. Zhu, J. A. Aguiar, J. A. Seabold, J. V. D. Lagemaat, H. M. Branz and N. R. Neale, *Nano Lett.*, 2015, **15**, 2517–2525.
20 S. Yang, X. Wen, W. Zhang and S. Yang, *J. Electrochem. Soc.*, 2005, **152**, 220-226.
21 A. B. Wong, S. Brittman, Y. Yu, N. P. Dasgupta and P. Yang, *Nano Lett.*, 2015, **15**, 4096–4101.
22 N. P. Dasgupta, J. Sun, C. Liu, S. Brittman, S. C. Andrews, J. Lim, H. Gao, R. Yan and P. Yang, *Adv. Mater.*, 2014, **26**, 2137–2184.
23 J. Tang, Z. Huo, S. Brittman, H. Gao and P. Yang, *Nat. Nanotechnol.*, 2011, **6**, 568–572.
24 W. Sheng, B. Sun, T. Shi, X. Tan, Z. Peng and G. Liao, *ACS Nano*, 2014, **8**, 7163–7169.
25 X. Zhao, P. Wang and B. Li, *Chem. Commun.*, 2010, **46**, 6768–6770.
26 M. Zhong, Y. Li, I. Yamada and J. J. Delaunay, *Nanoscale*, 2012, **4**, 1509–1514.
27 Q. B. Wu, S. Ren, S. Z. Deng, J. Chen and N. S. Xu, *J. Vac. Sci. Technol. B*, 2004, **22**, 1282-1285.
28 S. H. Wang and S. H. Yang, *Chem. Phys. Lett.*, 2000, **322**, 567–571.
29 S. H. Wang and S. H. Yang, *Chem. Mater.*, 2001, **13**, 4794–4799.
30 X. Liu, M. T. Mayer and D. Wang, *Angew. Chem. Int. Ed.*, 2010, **49**, 3165–3168.
31 L. Li, Z. Liu, M. Li, L. Hong, H. Shen, C. Liang, H. Huang, D. Jiang and S. Ren, *J. Phys. Chem. C*, 2013, **117**, 4253–4259.
32 U. Sim, J. Moon, J. An, J. H. Kang, S. E. Jerng, J. Moon, S. P. Cho, B. H. Hong and K. T. Nam, *Energy Environ. Sci.*, 2015, **8**, 1329–1338.
33 C. Xie, B. Nie, L. Zeng, F. X. Liang, M. Z. Wang, L. Luo, M. Feng, Y. Yu, C. Y. Wu, Y. Wu and S. H. Yu, *ACS Nano*, 2014, **8**, 4015-4022.
34 H. Li, X. Zhang and D. R. MacFarlane, *Adv. Energy Mater.*, 2015, **5**, 1401077.
35 J. Bian, C. Huang, L. Wang, T. Hung, W. A. Daoud and R. Zhang, *ACS Appl. Mater. Interf.*, 2014, **6**, 4883–4890.
36 X. Zhang, F. Wang, H. Huang, H. Li, X. Han, Y. Liu and Z. Kang, *Nanoscale*, 2013, **5**, 2274–2278.
37 X. Zhang, H. Huang, J. Liu, Y. Liu and Z. Kang, *J. Mater. Chem. A*, 2013, **1**, 11529-11533.
38 H. Yu, Y. Zhao, C. Zhou, L. Shang, Y. Peng, Y. Cao, L. Z. Wu, C. H. Tung and T. Zhang, *J. Mater. Chem. A*, 2014, **2**, 3344–3351
39 S. Xie, H. Su, W. Wei, M. Li, Y. Tong and Z. Mao, *J. Mater. Chem. A*, 2014, **2**, 16365–16368.
40 F. Nan, Z. Kang, J. Wang, M. Shen and L. Fang, *Appl. Phys. Lett.*, 2015, **106**, 153901.
41 F. Wang, Y. Liu, Z. Ma, H. Li, Z. Kang and M. Shen, *New J. Chem.*, 2013, **37**, 290–294
42 Y. Sun, Z. Zhang, A. Xie, C. Xiao, S. Li, F. Huang and Y. Shen, *Nanoscale*, 2015, **7**, 13974–13980.
43 J. Liu, Y. Liu, N. Y. Liu, Y. Z. Han, X. Zhang, H. Huang, Y. Lifshitz, S. T. Lee, J. Zhong and Z. H. Kang, *Science*, 2015, **347**, 970–974.
44 Y. Su, M. Xie, X. Lu, H. Wei, H. Geng, Z. Yang and Y. Zhang, *RSC Adv.*, 2014, **4**, 4839–4842.
45 H. Y. H. Chan, C. G. Takoudis and M. J. Weaver, *J. Phys. Chem. B.*, 1999, **103**, 357–365.
46 G. Lefvre, A. Walcarius, J. J. Ehrhardt and J. Bessire, *Langmuir*, 2000, **16**, 4519–4527.
47 J. F. Xu, W. Ji, Z. X. Shen, W. S. Li, S. H. Tang, X. R. Ye, D. Z. Jia and X. Q. Xin, *J. Raman Spectrosc.*, 1999, **30**, 413–415.
48. S. L. Diedenhofen, O. T. A. Janssen, G. Grzela, E. P. A. M. Bakkers and J. G. Rivas, *ACS Nano*, 2011, **5**, 2316–2323.
49 X. Yu, R. Liu, G. Zhang and H. Cao, *Nanotechnology*, 2013, **24**, 335401.
50 A. Kargar, Y. Jing, S. J. Kim, C. T. Riley, X. Pan and D. Wang, *ACS Nano*, 2013, **7**, 11112–11120.
51 J. Tang, Y. Zhang, B. Kong, Y. Wang, P. Da, J. Li, A. A. Elzatahry, D. Zhao, X. Gong and G. Zheng, *Nano Lett.*, 2014, **14**, 2702–2708.
52 M. G. Walter, E. L. Warren, J. R. McKone, S. W. Boettcher, Q. Mi, E. A. Santori and N. S. Lewis, *Chem. Rev.*, 2010, **110**, 6446–6473.
53 W. Y. Cheng, T. H. Yu, K. J. Chao and S. Y. Lu, *Int. J. Hydrogen Energy*, 2013, **38**, 9665–9672.
54 X. Li, H. Shen, S. Li, J. Z. Niu, H. Wang and L. S. Li, *J. Mater. Chem.*, 2010, **20**, 923–928.
55 A. A. Dubale, C. J. Pan, A. G. Tamirat, H. M. Chen, W. N. Su, C. H. Chen, J. Rick, D. W. Ayele, B. A. Aragaw, J. F. Lee, Y. W. Yang and B. J. Hwang, *J. Mater. Chem. A*, 2015, **3**, 12482–12499.
56 V. J. Babu, S. Vempati, T. Uyar and S. Ramakrishna, *Phys. Chem. Chem. Phys.*, 2015, **17**, 2960–2986.
57 T. Unold and H. W. Schock, *Annu. Rev. Mater. Res.*, 2011, **41**, 297–321.
58 U. Rau and H. W. Schock, *Appl. Phys. A*, 1999, **69**, 131–147.
59 J. Han, X. Zong, X. Zhou and C. Li, *RSC Adv.*, 2015, **5**, 10790–10794.
60 K. D. Lee, M. J. Park, D. Y. Kim, S. M. Kim, B. Kang, S. Kim, H. Kim, H. S. Lee, Y. Kang, S. S. Yoon, B. H. Hong and D. Kim, *ACS Appl. Mater. Interf.*, 2015, **7**, 19043–19049.